

Boundary damage effects on the evolution of creep strain

J Gullickson¹, A Needleman¹, A Staroselsky² and B Cassenti³

¹ Brown University, Division of Engineering, Providence, RI 02912, USA

² Pratt and Whitney, 400 Main Street, East Hartford, CT 06108, USA

³ Rensselaer Polytechnic Institute, 275 Windsor St, Hartford, CT 06120, USA

Received 30 November 2007, in final form 16 June 2008

Published 8 September 2008

Online at stacks.iop.org/MSMSE/16/075009

Abstract

The effect of a reduced section thickness leading to creep strain greater than that observed in the creep response of thicker sections is termed the thickness debit effect. We carry out three-dimensional analyses of the creep response of specimens with rectangular cross sections under uniaxial tensile loading having a boundary damage layer and explore whether this can account for the thickness debit effect. The particular damage mechanism modeled is plastic void nucleation, growth and coalescence with void nucleation taken to be confined to a surface layer and the material characterized as an elastic-power law creeping solid. Three-dimensional transient analyses are carried out but used to simulate quasi-static loading conditions. Results are presented for the effect of the thickness of the boundary damage layer on the creep response. The effect of varying the parameters characterizing the void nucleation process is also investigated. The results qualitatively exhibit a variety of features of the thickness debit effect seen in experiments.

(Some figures in this article are in colour only in the electronic version)

1. Introduction

As turbine design advances, the cooling passages in the superalloy turbine airfoils become increasingly complex, thus necessitating castings with significantly reduced thicknesses. There is experimental evidence, for example [1–5], that, at least in some cases, the reduced section thickness leads to superalloy creep deformation greater than what would be predicted based on the creep response of thicker sections. This is referred to as the thickness debit effect. Figure 1 shows creep strain data from Seetharaman and Cetel [5] illustrating the thickness debit. Curves of creep strain versus time are shown for single crystal sheet specimens of a nickel-based superalloy at an applied load (force/unit original area) with values of the sheet thickness varying by nearly an order of magnitude. The more rapid accumulation of creep strain for the thinner specimens is evident.

Baldan [4] argued that the creep response is controlled by the crack size to section size ratio. He presumed that the damage mechanism responsible for the thickness debit effect

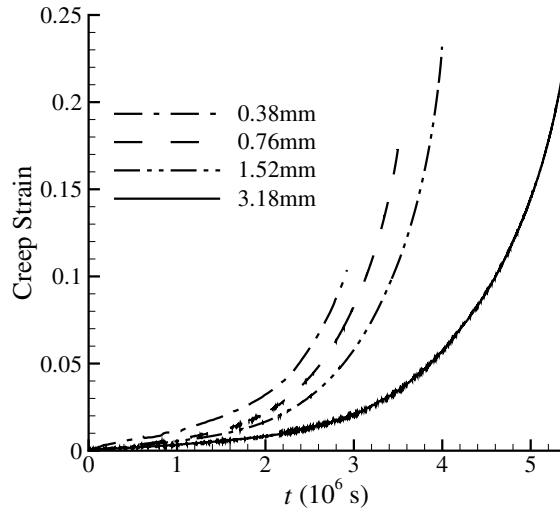


Figure 1. Effect of specimen thickness w on the creep strain versus time t for sheet specimens tested at 871 °C with an applied load of 413 MPa. Data from Seetharaman and Cetel [5].

occurred throughout the section. Seetharaman and Cetel [5] considered several possible explanations including cavity nucleation, growth and coalescence; oxygen embrittlement due to stress assisted grain boundary diffusion; and changes in anisotropy with section thickness.

Constitutive modeling of creep rupture has focused on the development of models for polycrystalline materials where grain boundary diffusion plays a prominent role as in [6–9]. However such a mechanism is not relevant for single crystal superalloys. The scenario we model is one in which surface defects lead to enhanced damage evolution in a surface layer with the specific damage mechanism being plastic void nucleation, growth and coalescence. Any possible diffusional contribution to void growth is neglected. The size of the damaged layer is assumed to be material specific and not to depend on the loading scheme or the specimen geometry. We examine the implications of such a damaged surface region for the observed thickness debit effect.

Three-dimensional analyses are carried out using the constitutive relation for progressively cavitating plastic solids due to Gurson [10] with the modified flow potential of Tvergaard [11, 12] and with the matrix material elastic–viscoplastic (Pan *et al* [13]). Isothermal conditions are assumed, the material parameters are chosen so to represent power law creep of the matrix and void nucleation is taken to be confined to a surface layer. The interior of the material is void free. Full transient analyses are carried out but used to simulate quasi-static loading conditions. Our focus is on the effect of the ratio of surface layer thickness to specimen size on the evolution of the creep strain.

2. Formulation

2.1. Governing equations

The finite element calculations are based on the dynamic principle of virtual work, as in [16] which is written as

$$\int_V \tau^{ij} \delta E_{ij} dV = \int_S T^i \delta u_i dS - \int_V \rho \frac{\partial^2 u^i}{\partial t^2} \delta u_i dV \quad (1)$$

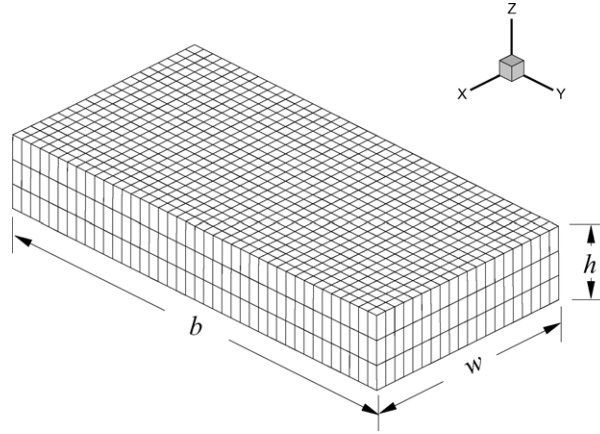


Figure 2. The specimen analyzed in most of the calculations with the finite element mesh used. Here and in subsequent figures (X, Y, Z) correspond to (x^1, x^2, x^3) .

with

$$T^i = (\tau^{ij} + \tau^{kj} u_{,k}^i) v_j, \quad E_{ij} = \frac{1}{2}(u_{i,j} + u_{j,i} + u_i^k u_{k,j}), \quad (2)$$

where τ^{ij} are the contravariant components of Kirchoff stress on the deformed convected coordinate net, u_j are the covariant components of the displacement vector, v_j are the covariant components of the reference surface normal, ρ is the mass density, V and S are the volume and surface of the body in the reference configuration and $(\cdot)_{,i}$ denotes covariant differentiation in the reference frame.

The specimen analyzed has dimensions $2w \times 2b \times 2h$. Symmetry conditions are assumed so that the region analyzed, and shown in figure 2, is $0 \leq x^1 \leq w$, $0 \leq x^2 \leq b$ and $0 \leq x^3 \leq h$. As in the load controlled experiments of Seetharaman and Cetel [5], a nominal traction (force/unit initial area) rather than a true traction is prescribed. The tensile loading is imposed on the surface $x^3 = h$ which remains shear free so that

$$T^3(x^1, x^2, h) = T_{\text{appl}}, \quad T^1(x^1, x^2, h) = T^2(x^1, x^2, h) = 0. \quad (3)$$

The symmetry conditions on $x^3 = 0$ are

$$u_3(x^1, x^2, 0) = 0, \quad T^1(x^1, x^2, 0) = 0, \quad T^2(x^1, x^2, 0) = 0. \quad (4)$$

Traction free conditions are prescribed on $x^1 = w$ and $x^2 = b$ and symmetry conditions on $x^1 = 0$ and $x^2 = 0$

$$u_1(0, x^2, x^3) = 0, \quad T^2(0, x^2, x^3) = 0, \quad T^3(0, x^2, x^3) = 0. \quad (5)$$

$$u_2(x^1, 0, x^3) = 0, \quad T^1(x^1, 0, x^3) = 0, \quad T^3(x^1, 0, x^3) = 0, \quad (6)$$

2.2. Constitutive relation

The constitutive relation used for the specimen is a modified Gurson [10–13] constitutive relation for a progressively cavitating plastic solid that has been extensively used to model ductile damage and will only be briefly outlined here. Background on this constitutive relation and further details are given in Tvergaard [14] and Needleman *et al* [15].

The rate of deformation tensor is written as the sum of the elastic part d^e and a viscoplastic part d^p

$$d = d^e + d^p, \quad d^e = L^{-1} : \hat{\sigma}. \quad (7)$$

Here, $\hat{\sigma}$ is the Jaumann rate of Cauchy stress. We assume elastic isotropy and small elastic strains. The tensor of elastic moduli \mathbf{L} is then given by

$$\mathbf{L} = \frac{E}{1+\nu} \left(\mathbf{I}' + \frac{\nu}{1-2\nu} \mathbf{I} \otimes \mathbf{I} \right), \quad (8)$$

where \mathbf{I} and \mathbf{I}' are the second and fourth order identity tensors, respectively. The material properties used are: $E = 200$ GPa, $\nu = 0.3$ and $\rho = 10^3 \text{ kg m}^{-2} = 10^{-2} \text{ MPa (m/s)}^{-2}$.

The plastic strain rate is given by

$$\mathbf{d}^p = \left[\begin{array}{c} (1-f)\bar{\sigma}\dot{\bar{\epsilon}} \\ \sigma : \frac{\partial \Phi}{\partial \sigma} \end{array} \right] \frac{\partial \Phi}{\partial \sigma} \quad (9)$$

with the flow potential having the form

$$\Phi = \frac{\sigma_e^2}{\bar{\sigma}^2} + 2q_1 f \cosh\left(\frac{3q_2 \sigma_h}{2\bar{\sigma}}\right) - 1 - (q_1 f)^2 = 0. \quad (10)$$

In these equations, f is the void volume fraction, q_1 and q_2 , Tvergaard [11, 12], are constants (with $q_1 = 1.25$ and $q_2 = 1$ in the calculations here), σ_e is the Mises effective stress and σ_h is the mean normal stress (the hydrostatic tension), given by

$$\sigma_e^2 = \frac{3}{2} \sigma' : \sigma', \quad \sigma_h = \frac{1}{3} \sigma : \mathbf{I}, \quad \sigma' = \sigma - \sigma_h \mathbf{I}. \quad (11)$$

The matrix plastic strain rate, $\dot{\bar{\epsilon}}$, is given by power hardening law as follows:

$$\dot{\bar{\epsilon}} = \dot{\epsilon}_0 \left[\frac{\bar{\sigma}}{g(\bar{\epsilon})} \right]^{1/m}, \quad g(\bar{\epsilon}) = \sigma_0 [1 + \bar{\epsilon}/\epsilon_0]^N. \quad (12)$$

Since the aim is to model quasi-static loading, the material properties and dimensions are specified in terms of relevant dimensionless ratios. All calculations are carried out using $\epsilon_0 = \sigma_0/E = 0.0025$. The rate hardening exponent m is taken to be $m = 1/5$ and $N = 0.001$ (essentially non-hardening) to approximate power law creeping behavior. Also, the effective yield stress was chosen to be $\sigma_0 = 2T_{\text{appl}}$ where T_{appl} is the applied traction in equation (3) giving $\dot{\bar{\epsilon}}/\dot{\epsilon}_0 = (T_{\text{appl}}/\sigma_0)^{1/m} = 0.871$.

The evolution of the void volume fraction is governed by

$$\dot{f} = (1-f)\mathbf{d}^p : \mathbf{I} + \dot{f}_{\text{nucl}}, \quad (13)$$

where the first term on the right hand side accounts for void growth and the second term for void nucleation. Void nucleation is taken to be strain controlled with a normal distribution (Chu and Needleman [17]), with

$$\dot{f}_{\text{nucl}} = D\dot{\bar{\epsilon}}D = \frac{f_N}{s_N\sqrt{2\pi}} \exp\left[-\frac{1}{2}\left(\frac{\bar{\epsilon} - \epsilon_N}{s_N}\right)^2\right], \quad (14)$$

where f_N is value of the volume fraction of voids available for nucleation, ϵ_N is the mean void nucleation strain and s_N is the corresponding standard deviation.

2.3. Numerical Implementation

An explicit dynamic analysis is carried out in order to avoid forming a large three-dimensional finite element stiffness matrix. The parameters associated with the dynamics (the density, loading rate, etc) are chosen so as to minimize dynamic effects and approximate quasi-static response. Essentially, the technique is one of dynamic relaxation.

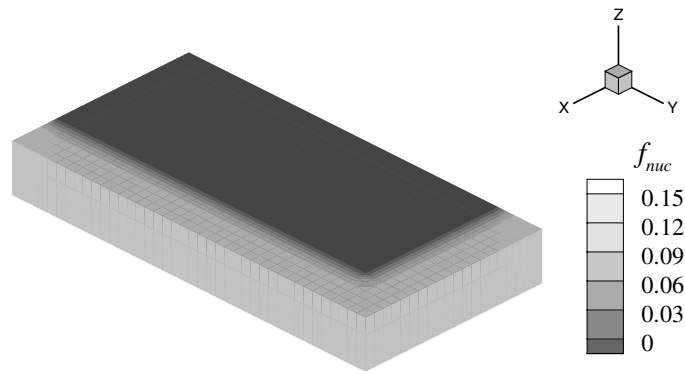


Figure 3. Contour plot showing the surface layer in the specimen where voids can nucleate and grow. The geometry shown has $s = 0.2w$.

Twenty node brick elements are used with eight point integration. The resulting equations of motion are integrated numerically by an explicit integration procedure, the Newmark β -method with $\beta = 0$, Belytschko [18]. The rate tangent method of Peirce *et al* [19] is used for constitutive updating.

A representative region analyzed is shown in figure 3. The possibility of damage nucleation in the form of voids is shown here with contours of f_{nuc} . The material where damage due to void nucleation and growth is possible is confined to a surface layer. Interior to this boundary layer is the bulk material where no voids are allowed to develop.

Under quasi-static loading conditions, and prior to any localization instability, field quantities are independent of x^3 . Thus, in most calculations a relatively thin slice having $h = 0.25w$ is analyzed. For comparison purposes, some calculations were carried out with $h = 2w$. As will be shown subsequently, the computed response is essentially the same for both values of h .

The thickness of the boundary layer, s , where damage occurs was varied between 10% and 40% of the smallest dimension, w . For all calculations with $h = 0.25w$, the number of elements and the element dimensions are fixed. Results are presented for $s = 0.1w$, $s = 0.2w$ and $s = 0.4w$. A $40 \times 20 \times 3$ element mesh is used which has 2400 20-node brick elements and 38001 degrees of freedom. With this mesh $s = 0.1w$, $s = 0.2w$ and $s = 0.4w$ comprise two, four and eight element widths, respectively.

3. Numerical results

Calculations are carried out for three values of the ratio of the thickness of the damaged boundary layer s to specimen half-width w ; $s/w = 0.1, 0.2$ and 0.4 using the reference values $f_N = 0.04$, $s_N = 0.01$ and $\epsilon_N = 0.1$. Parameter studies were carried out varying the value of the void nucleation strain ϵ_N and the value of the volume fraction of voids available for nucleation f_N . Specifically, the values $\epsilon_N = 0.025$ and $\epsilon_N = 0.05$, and $f_N = 0.08$ and $f_N = 0.16$ are used in addition to the reference values. In addition, calculations are carried out for two values of the initial strain rate $\dot{\epsilon}_0$, a reference value $\dot{\epsilon}_{0ref}$ and a value an order of magnitude larger $10\dot{\epsilon}_{0ref}$. In both cases, since $(T_{appl}/\sigma_0) = 1/2$, $\dot{\epsilon}/\dot{\epsilon}_{0ref} = 0.871$. All calculations are continued to a true strain of 0.20, defined as the logarithmic $\epsilon_{true} = \ln(1 + u_3(0, 0, h)/L)$. The value of the true strain is minimum at $(0, 0, h)$ and the maximum variation along the surface $x^3 = h$ is less than 0.4%.

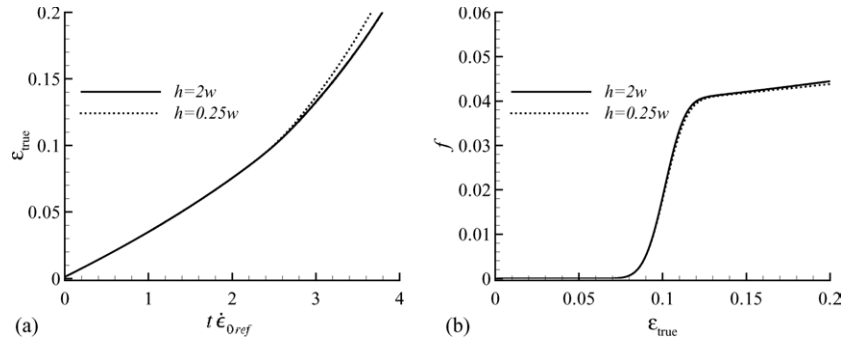


Figure 4. (a) True strain ϵ_{true} as a function of the normalized time $t\dot{\epsilon}_{0\text{ref}}$. (b) Void volume fraction f versus true strain ϵ_{true} . Results from calculations with $h = 2w$ and $h = 0.25w$ are compared for $s = 0.4w$ and the reference values of the void nucleation parameters as stated in the text.

To investigate the variation with the height of the region analyzed, a calculation was carried out with $h = 2w$ as well as $h = 0.25w$. For both calculations the surface layer thickness was $s = 0.4w$ and the reference values of the void nucleation parameters were used. The same mesh spacing was used for both values of h so that with $h = 2w$ there are eight times as many finite elements as with $h = 0.25w$ and, accordingly, a factor of eight increase in computation time.

Figure 4(a) shows curves of true strain ϵ_{true} versus normalized time $\dot{\epsilon}_{0\text{ref}}t$ for specimen heights of $h = 2w$ and $h = 0.25w$ using the reference material parameters. Up to a true strain of about 0.12, the results for the two values of h essentially coincide. For larger strains (up to 0.2 which is the maximum strain of interest here) there is a small difference, but the qualitative features of the behavior are the same and the quantitative difference is small. Figure 4(b) shows the void volume fraction versus true strain behavior for specimen heights of $h = 2w$ and $h = 0.25w$. There is no difference in the response with the two values of h prior to the nucleation of voids and even after voids have nucleated essentially the same curve of void volume fraction f versus true strain ϵ_{true} is obtained for both $h = 2w$ and $h = 0.25w$.

Contours of void volume fraction at $\epsilon_{\text{true}} = 0.2$ are shown in figure 5. The contours of void volume fraction are not affected by specimen height. For both cases, the void volume fraction is at a constant maximum of $f = 0.04$ throughout the surface layer, and the bulk material has no voids. Variations between the surface layer and the bulk material are due to interpolation of f onto the finite element mesh.

Figure 6 shows contours of Mises effective stress at $\epsilon_{\text{true}} = 0.2$. The stress level is somewhat lower in the shorter specimen, $h = 0.25w$. The maximum difference in stress magnitude is approximately 3% at any point through the thickness. The distributions of Mises effective stress are qualitatively similar in both cases with the highest stress magnitude in the surface damage layer with a stress maximum at the corner (w, b, h) and a stress minimum in the bulk.

3.1. Parameter studies

Figure 7 shows the variation of ϵ_{true} with dimensionless time, $t\dot{\epsilon}_{0\text{ref}}$ for three values of the boundary damage layer thickness, $s = 0.1w$, $s = 0.2w$ and $s = 0.4w$. Increasing f_N decreases the creep time necessary to reach a true strain of 0.2 for all three values of the boundary damage layer thickness.

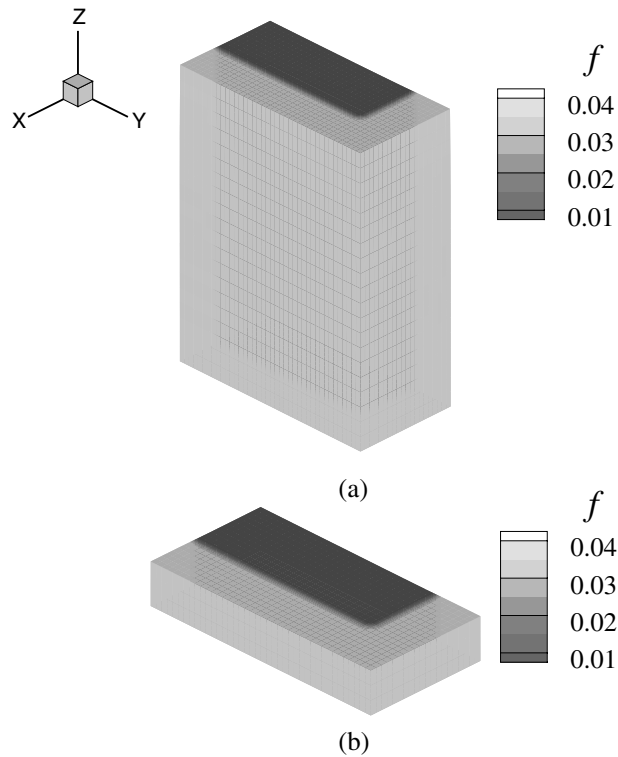


Figure 5. Contours of void volume fraction at $\epsilon_{\text{true}} = 0.2$ for (a) $h = 2w$ and (b) $h = 0.25w$ with $s = 0.4w$ and the reference values of the void nucleation parameters as stated in the text.

Increasing the relative width of the boundary damage layer s from $0.1w$ to $0.4w$ decreases the normalized time required to reach $\epsilon_{\text{true}} = 0.2$. As the amplitude of the void nucleation function, f_{N} , is increased, the effect of the boundary damage layer thickness also increases: for example, with $f_{\text{N}} = 0.04$ and $\epsilon_{\text{N}} = 0.035$, $t\dot{\epsilon}_{0\text{ref}} = 3.40$ for $s = 0.1w$ and $t\dot{\epsilon}_{0\text{ref}} = 3.20$ for $s = 0.4w$. The thickness debit effect is enhanced for smaller values of ϵ_{N} .

Figure 8 shows curves of void volume fraction f versus true strain ϵ_{true} for the calculations with (a) $\epsilon_{\text{N}} = 0.025$ and (b) $\epsilon_{\text{N}} = 0.10$. Calculations, not shown here, were also carried out with $\epsilon_{\text{N}} = 0.05$ and those results exhibit the same trends as those with $\epsilon_{\text{N}} = 0.025$ and $\epsilon_{\text{N}} = 0.10$. The value of the amplitude of the void nucleation function, f_{N} , has the largest effect on the void volume fraction versus true strain response for each value of ϵ_{N} . As f_{N} increases, the value of the volume fraction of voids, f , attained after $\epsilon_{\text{true}} = \epsilon_{\text{N}}$ increases accordingly.

The evolution of the void volume fraction f in figure 8 shows that there is very little void growth after nucleation. Thus, the effect of damage on the creep rate arises from void nucleation rather than from void growth. This is expected as the stress triaxiality is low ($1/3$) for uniaxial stressing and void growth is strongly affected by the stress triaxiality. Figures 7 and 8 show that as the void nucleation strain, ϵ_{N} , decreases the effect of both the boundary damage layer thickness, s and the amplitude of the strain nucleation function f_{N} become more pronounced.

Figures 9 and 10 show contours of (a) σ_e and (b) f for the calculations with $\epsilon_{\text{N}} = 0.1$ and $f_{\text{N}} = 0.04$ at $\epsilon_{\text{true}} = 0.2$ with $s = 0.1w$ and $s = 0.4w$, respectively. These

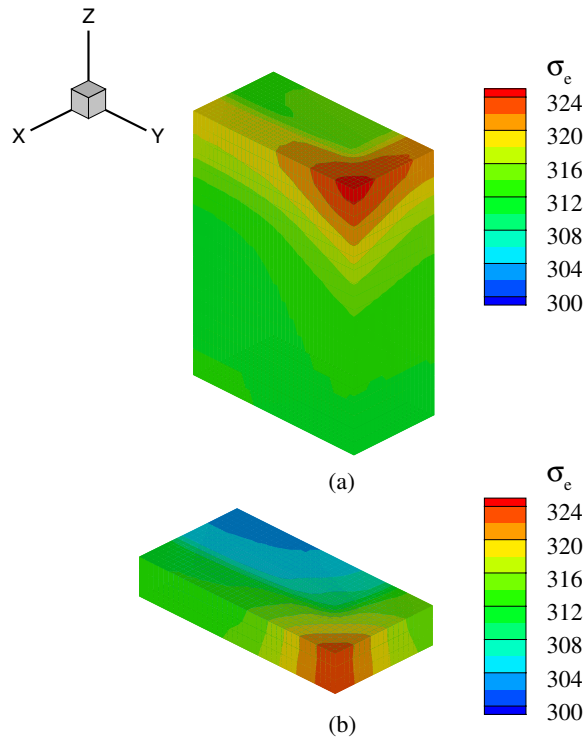


Figure 6. Contours of Mises effective stress σ_e at $\epsilon_{true} = 0.2$ for (a) $h = 2w$ and (b) $h = 0.25w$ with $s = 0.4w$ and the reference properties.

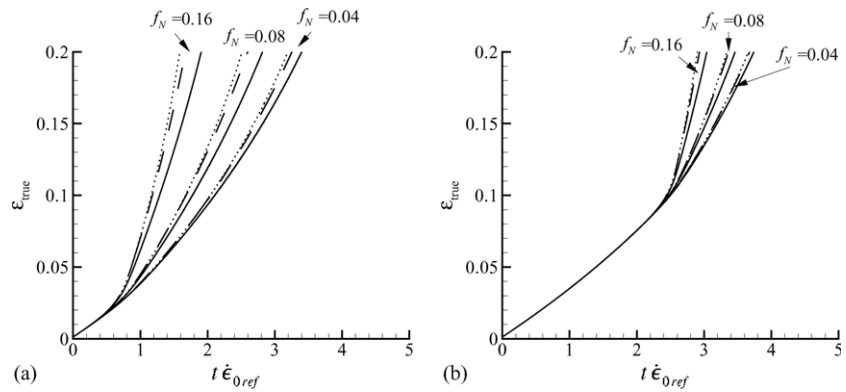


Figure 7. True strain ϵ_{true} versus $t\dot{\epsilon}_{0ref}$ for the calculations with varying nucleation parameters f_N and ϵ_N and varying wall width s . Solid, dashed and dotted lines correspond to surface layer thicknesses of $s = 0.1w$, $s = 0.2w$ and $s = 0.4w$, respectively. (a) $\epsilon_N = 0.025$, (b) $\epsilon_N = 0.1$.

contours are representative, with the region where voids have nucleated and are growing encompassing the entire boundary damage layer. In the boundary damage layer where the void volume fraction is at a maximum, the Mises effective stress, σ_e is at a maximum. The levels of Mises effective stress in the specimen are higher for the thicker boundary layer.

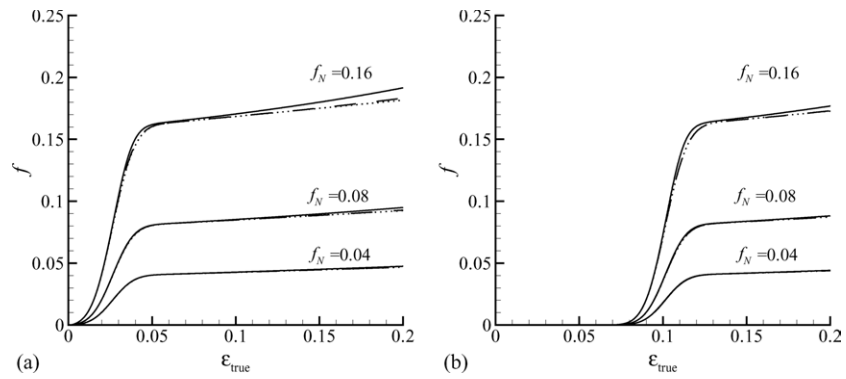


Figure 8. Void volume fraction f versus true strain ϵ_{true} for the calculations with varying nucleation parameter f_N and ϵ_N and varying wall width s . Solid, dashed and dotted lines correspond to surface layer thicknesses of $s = 0.1w$, $s = 0.2w$ and $s = 0.4w$, respectively. (a) $\epsilon_N = 0.025$, (b) $\epsilon_N = 0.10$.

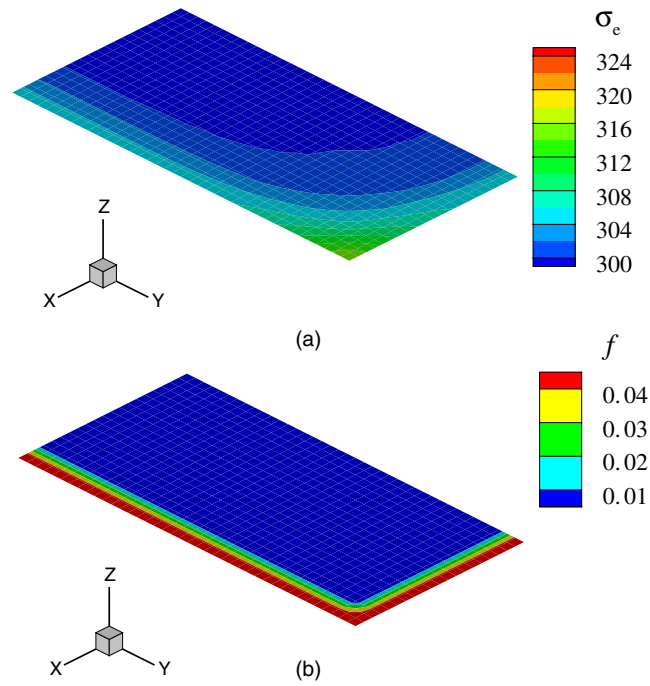


Figure 9. Contours at $x^3 = h/2$ and $\epsilon_{\text{true}} = 0.2$ of (a) Mises effective stress, σ_e , and (b) void volume fraction, f for the reference values of the void nucleation parameters as stated in the text and with $s = 0.1w$.

Calculations were carried out for two values of $\dot{\epsilon}_0$, the reference value and a value 10 times larger. Since for the materials of interest here, increasing the ambient temperature increases the creep rate, increasing $\dot{\epsilon}_0$ provides a simple way within the context of a purely mechanical theory of exploring the implications of this. Also, for pure power law creep behavior and under constant load, increasing $\dot{\epsilon}_0$ is approximately the same as increasing T_{appl} .

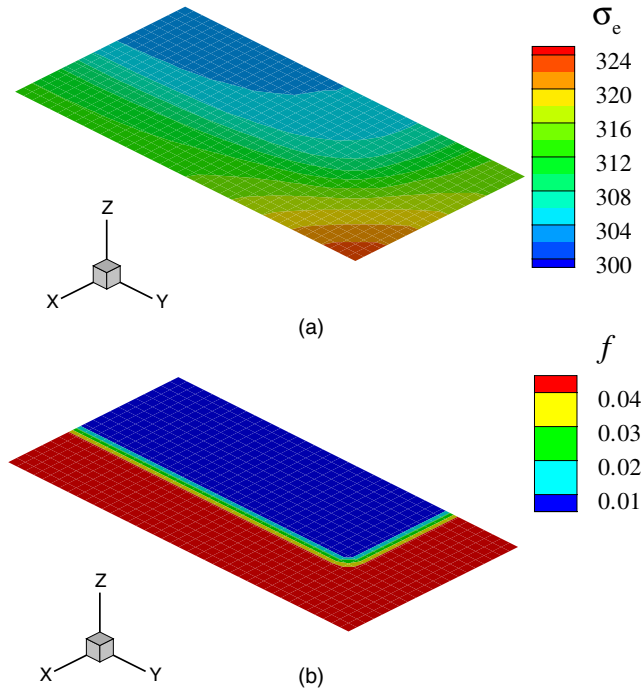


Figure 10. Contours at $x^3 = h/2$ and $\epsilon_{\text{true}} = 0.2$ of (a) Mises effective stress, σ_e , and (b) void volume fraction, f for the reference values of the void nucleation parameters as stated in the text and with $s = 0.4w$.

Figure 11 shows the true strain ϵ_{true} versus normalized time $t\dot{\epsilon}_{0\text{ref}}$ response with $\dot{\epsilon}_0 = \dot{\epsilon}_{0\text{ref}}$ and $\dot{\epsilon}_0 = 10\dot{\epsilon}_{0\text{ref}}$. Increasing the initial strain rate, $\dot{\epsilon}_0$, by a factor of 10 causes a significant decrease in the time to attain a given value of ϵ_{true} . In fact, there is essentially a linear scaling with the value of $\dot{\epsilon}_0$. This is seen more clearly in figure 12 which shows the variation of normalized time, $t\dot{\epsilon}_0 = \dot{\epsilon}_{0\text{ref}}$, to reach $\epsilon_{\text{true}} = 0.15$ with the relative thickness of the boundary damage layer, w/s . With $\dot{\epsilon}_0 = 10\dot{\epsilon}_{0\text{ref}}$, figure 12(b), the absolute value of the thickness debit effect is decreased by an order of magnitude compared with that in figure 12(a), i.e. in proportion to the variation in $\dot{\epsilon}_0$.

4. Discussion

Our numerical results show that a surface damage layer can lead to size dependent creep behavior that is qualitatively consistent with experimental observations. The calculations employ a constitutive relation modeling plastic void nucleation, growth and coalescence. For polycrystalline metals at high temperatures models have been developed for diffusion assisted creep void nucleation and growth [20–22]. While it is possible that diffusion plays a role in the thickness debit effect, the mechanism, and therefore the modeling required, will be different from that for polycrystalline metals. For a power law creeping solid, Van der Giessen *et al* [21] shows that for cavity growth without diffusion void growth rates increase rapidly with increasing stress triaxiality, and at low stress triaxiality the influence of the void volume fraction on void growth rate is small. We find (see figure 11) that for power law creep it is void nucleation rather than void growth that controls to the enhanced creep rate. Komenda and

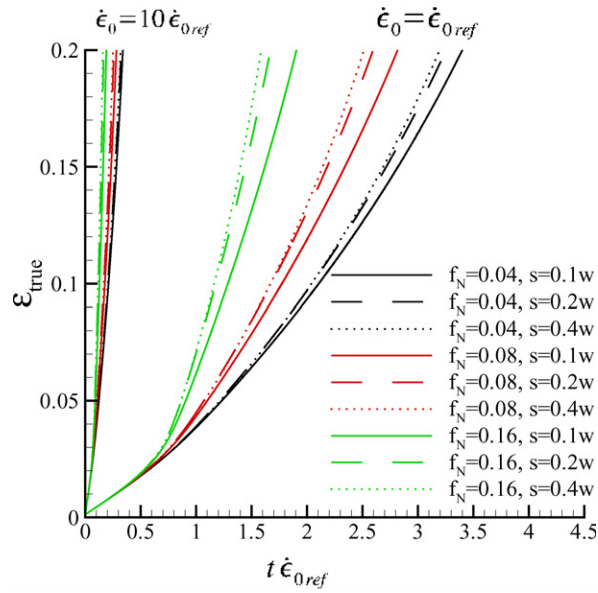


Figure 11. True strain ϵ_{true} normalized creep time $t\dot{\epsilon}_{0\text{ref}}$ for the three values of s/w , three values of the amplitude of the void nucleation function f_N and for $\dot{\epsilon}_0 = \dot{\epsilon}_{0\text{ref}}$ and $\dot{\epsilon}_0 = 10\dot{\epsilon}_{0\text{ref}}$. The void nucleation strain is $\epsilon_N = 0.025$.

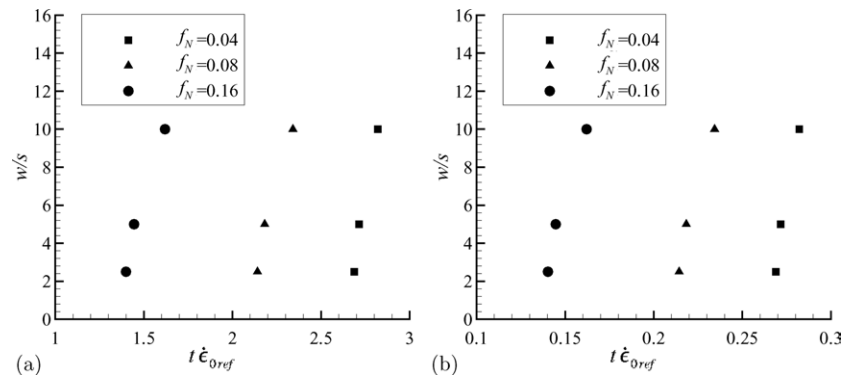


Figure 12. Normalized thickness, w/s versus normalized creep time to $\epsilon_{\text{true}} = 0.15$, for the three boundary layer thicknesses. The parameters $\epsilon_N = 0.025$ and $f_N = 0.04, 0.08$ and 0.16 are used with (a) $\dot{\epsilon}_0 = \dot{\epsilon}_{0\text{ref}}$ and (b) $\dot{\epsilon}_0 = 10\dot{\epsilon}_{0\text{ref}}$.

Henderson [23] presume that the voids they see in their experimental study are pre-existing and that void nucleation does not play a role. Calculations with pre-existing voids can be carried out within the framework we have used but it is expected that the results would not differ significantly from those with a small nucleation strain. As seen in the results from [21], the very low void growth rate is a consequence of the low value of stress triaxiality in the uniaxial stress state that prevails in the specimens. Hence, the thickness debit seen in the calculations is most likely not dependent on the details of our damage model; any surface boundary layer damage mechanism that comes into play at a given strain would exhibit similar behavior.

Baldan [4] argued that damage in the form of micro-cracks leading to voids throughout the specimen was responsible for limiting the creep lifetime of nickel-based superalloy components and for the thickness debit effect. In order to explore this within the framework of our model, we carried out calculations with damage occurring throughout the specimen for two values of specimen thickness; w , the value used in all calculations presented here, and a thickness $w/2$. The creep strain versus time curves for these two calculations were nearly identical. Also, these creep strain versus time curves were very close to those presented here with $s = 0.4w$. Thus, at least within the framework of the ductile damage model used here, the development of damage throughout the specimen, rather than in a surface boundary layer, does not explain the thickness debit effect.

To give some idea of the thicknesses involved we relate the ratios used in the numerical results to the dimensions used in the experiments. For the experimental results shown in figure 1, $s/w = 0.4$ corresponds to a damage boundary layer thickness of $152 \mu\text{m}$ for the specimen with $w = 0.38 \text{ mm}$. With this damage boundary layer thickness, the ratio of damage boundary layer thickness to specimen width is 0.1 for the specimen with $w = 1.52 \text{ mm}$.

The thickness debit effect is seen for all values of the void nucleation parameters considered here. An increased value of the volume fraction of voids that can be nucleated, f_N , decreases the time to attain a specified creep strain. A smaller value of the void nucleation strain ϵ_N results in an increased magnitude of the thickness debit.

For pure power law creep constitutive behavior, $\dot{\epsilon} \propto \dot{\epsilon}_0$ and the numerical results here follow that scaling very closely even though due to porosity the plastic response is not exactly that of pure power law creep and also a fixed nominal rather than fixed true traction is prescribed. Furthermore, for pure power law creep behavior, increasing $\dot{\epsilon}_0$ is equivalent to decreasing flow strength σ_0 . In general, σ_0 decreases with temperature (although anomalies do occur) and other material parameters may depend on temperature. Presuming that the main effect of temperature in the experiments of Seetharaman and Cetel [5] is through the temperature dependence of σ_0 , our results with the scaling factor $\dot{\epsilon}_0 = 10\dot{\epsilon}_{0\text{ref}}$ can be viewed as representing the predictions for an increased temperature and are qualitatively consistent with the experimental observations in Seetharaman and Cetel [5].

Figure 13 shows a qualitative comparison of the thickness debit effect in the experimental results of Seetharaman and Cetel [5] (the points) and lines given by a least squares linear fit to the results of the computations here. To make the comparison possible, the experimental results are normalized by an arbitrarily chosen reference thickness $w_0 = 0.3 \text{ mm}$ and by an arbitrarily chosen reference time t_0 that depends on the test temperature and applied load. Of course, the normalizations of the data are arbitrary but the trends are reasonably well represented by the calculations (note that although a linear fit to the computations is shown in figure 13, figure 12(a) shows that the computational results exhibit a similar curvature to that seen in the experiments). This comparison suggests that the mechanism of a boundary damage layer for the thickness debit effect is at least a plausible one.

5. Conclusions

- The thickness debit effect can be captured, at least qualitatively, by a model for the nucleation and growth of voids in a boundary damage layer.
- At least in the circumstances analyzed here, the effect of damage on the creep rate arises from void nucleation rather than from void growth.
- The creep response, and therefore the thickness debit effect, depends both on the boundary damage layer thickness and on the void nucleation parameters used in the analyses.

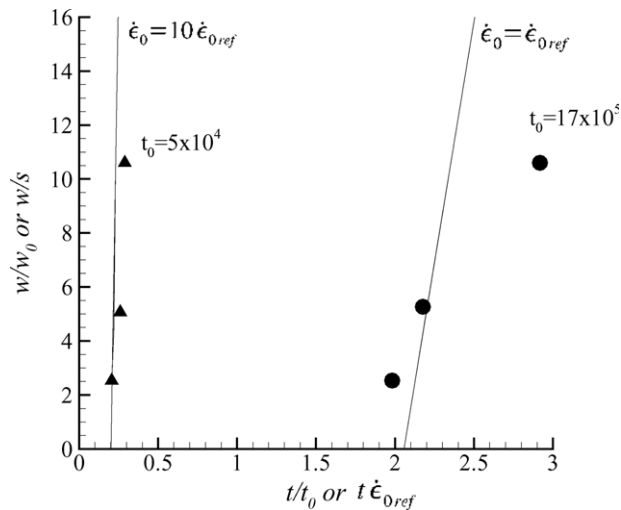


Figure 13. Comparison of experiment and computation for the thickness debit effect. The points are from Seetharaman and Cetel [5]. To enable the comparison the data points are normalized with w being the specimen width and $w_0 = 0.3$ mm, a reference width being 0.3 mm; t is the time to reach a strain of 0.15 and $t_0 = 17 \times 10^5$ s for the specimen tested at 413 MPa at 871 °C and $t_0 = 1 \times 10^4$ s for the specimen tested at 248 MPa and 982 °C. The lines are least square fits to the results in figure 12 for the calculations with $f_N = 0.08$.

- The thickness debit effect occurs for all values of the void nucleation parameters used here, but is more pronounced for larger values of the amplitude of nucleating voids, f_N , and smaller values of the mean nucleation strain, ϵ_N .
- The effect of increasing the value of the reference strain rate, $\dot{\epsilon}_0$ was explored as a simple model for estimating the effect of increasing temperature and/or increasing applied load. Increasing $\dot{\epsilon}_0$ caused an overall decrease in the creep time to a given true strain and an associated decrease in the magnitude of the thickness debit effect.

Acknowledgments

JG and AN are grateful for the support provided by Pratt & Whitney through the University Initiative Program.

References

- [1] Gibbons T B 1981 Creep properties of Nimonic 90 in thin section *Met. Technol.* **8** 472–5
- [2] Dyson B F 1983 Continuous cavity nucleation and creep fracture *Scr. Metall.* **17** 31–7
- [3] Pandey M C, Taplin D M R and Rao P R 1989 An analysis of specimen geometry effect on the creep life of inconel alloy X-750 *Mater. Sci. Eng. A—Struct. Mater. Properties Microstruct. Process.* **118** 33–9
- [4] Baldan A 1995 On the thin-section size dependent creep strength of a single crystal nickel-base superalloy *J. Mater. Sci.* **30** 6288–98
- [5] Seetharaman V and Cetel A D 2004 Thickness debit in creep properties of PWA 1484 *Superalloy 2004* ed K A Green *et al* (Warrendale, PA: Minerals, Metals and Materials Society) pp 207–14
- [6] Tvergaard V 1985 Effect of grain boundary sliding on creep constrained diffusive cavitation *J. Mech. Phys. Solids* **33** 447–69
- [7] Tvergaard V 1984 On the creep constrained diffusive cavitation of grain boundary facets *J. Mech. Phys. Solids* **32** 373–93

- [8] Van der Giessen E and Tvergaard V 1991 A creep-rupture model accounting for cavitation at sliding grain-boundaries *Int. J. Fract.* **48** 153–78
- [9] Van der Giessen E, Onck P R and Van der Burg M W D 1997 Some effects of random microstructural variations on creep rupture *Eng. Fract. Mech.* **57** 205–26
- [10] Gurson A L 1975 Plastic flow and fracture behavior of ductile materials incorporating void nucleation, growth and interaction *PhD Thesis* Brown University
- [11] Tvergaard V 1981 Influence of voids on shear band instabilities under plane strain conditions *Int. J. Fract.* **17** 389–407
- [12] Tvergaard V 1982 On localization in ductile materials containing spherical voids *Int. J. Fract.* **18** 237–52
- [13] Pan J, Saje M and Needleman A 1983 Localization of deformation in rate sensitive porous plastic solids *Int. J. Fract.* **21** 261–78
- [14] Tvergaard V 1990 Material failure by void growth to coalescence *Adv. Appl. Mech.* **27** 83–151
- [15] Needleman A, Tvergaard V and Hutchinson J W 1992 Void growth in plastic solids *Topics in Fracture and Fatigue* ed A S Argon (New York: Springer) pp 145–78
- [16] Tvergaard V and Needleman A 2006 Three dimensional microstructural effects on plane strain ductile crack growth *Int. J. Solids Struct.* **43** 6165–79
- [17] Chu C C and Needleman A 1980 Void nucleation effects in biaxially stretched sheets *J. Eng. Mater. Technol.* **102** 249–56
- [18] Belytschko T 1976 A survey of numerical methods and computer programs for dynamic structural analysis *Nucl. Eng. Des.* **37** 23–34
- [19] Peirce D, Shih C F and Needleman A 1984 A tangent modulus method for rate dependent solids *Comput. Struct.* **18** 875–87
- [20] Van der Giessen E and Tvergaard V 1996 Micromechanics of intergranular creep failure under cyclic loading *Acta Mater.* **44** 2697–710
- [21] Van der Giessen E, Van der Burg M W D, Needleman A and Tvergaard V 1995 Void growth due to creep and grain boundary diffusion at high triaxialities *J. Mech. Phys. Solids* **43** 123–65
- [22] Van der Giessen E and Tvergaard V 1994 Development of final creep failure in polycrystalline aggregates *Acta Metall. Mater.* **42** 959–73
- [23] Komenda J and Henderson P J 1997 Growth of pores during the creep of a single crystal nickel-base superalloy *Scr. Mater.* **37** 1821–6